

# Intra-DP: A High Performance Distributed Inference System on Robotic IoT

Anonymous Author(s)

Submission Id: 445

## Abstract

The rapid advancements in machine learning (ML) techniques have led to significant achievements in various robotic tasks, where deploying these ML approaches on real-world robots requires fast and energy-efficient inference of their deep neural network (DNN) models. Distributed inference, which involves inference across multiple powerful GPU devices, has emerged as a promising optimization to improve inference performance in modern data centers. However, when deployed over Internet of Things of these real-world robots (robotic IoT), all existing parallel methods (data parallelism, tensor parallelism, pipeline parallelism) fail to simultaneously meet the robots' latency and energy requirements and raise significant challenges due to the failure of data parallelism, the unacceptable communication overhead of tensor parallelism, and the significant transmission bottlenecks in pipeline parallelism due to the limited bandwidth of robotic IoT.

We present Intra-DP, the first high-performance distributed inference system optimized for model inference on robotic IoT. Intra-DP introduces a fine-grained approach to transmission and computation by confining them to each local operator of DNN layers (i.e., operators that can be computed independently without the complete input, such as the convolution kernel in the convolution layer). By adaptively scheduling the computation and transmission of each local operator based on various hardware conditions and network bandwidth, Intra-DP enables different local operators of different layers to be computed and transmitted concurrently, and overlap the computation and transmission phases within the same inference task to achieve fast and energy-efficient distributed inference on robotic IoT. The evaluation shows that Intra-DP reduces inference time by 20% and energy consumption by 10% compared to the state-of-the-art baselines.

**Keywords:** Distributed inference, Robotic IoT, Distributed system and network

## 1 Introduction

The rapid progress in machine learning (ML) techniques has led to remarkable achievements in various fundamental robotic tasks, such as object detection [20, 30, 33], robotic control [24, 50, 60], and environmental perception [4, 25, 55]. However, deploying these ML applications on real-world robots requires fast and energy-efficient inference of their deep neural network (DNN) models, given the need for swift

environmental responses and the limited battery capacity of robots. Placing the entire model on robots not only requires additional computing accelerators on robots (e.g., GPU [37], FPGA [38], SoC [16]), but also introduce additional energy consumption (e.g., 162% more for [33] in our experiments) due to the computationally intensive nature of DNN models, while placing the entire model in the cloud brings an extended response delay.

Distributed inference, which involves inference across multiple GPU devices, has emerged as a promising approach to meet the latency requirements of robotic applications and extend the battery lifetime of robots. This paradigm has been widely adopted in data centers [18, 56, 64], where numerous GPUs are utilized to speed large model inference, such as in the case of ChatGPT [54]. Adopting distributed inference across robots and other powerful GPU devices through the Internet of Things for these robots (robotic IoT) not only accelerates the inference process by leveraging the high computing capabilities of powerful GPUs but also alleviates the local computational burden, thereby reducing energy consumption, making it an ideal solution for robotic applications.

However, all existing parallel methods for distributed inference in the data center are ill-suited for robotic IoT. In data centers, there are mainly three kinds of parallel methods: Data parallelism (DP) replicates the model across devices, and lets each replica handle one mini-batch (i.e., a subset that slices out of an input data set); Tensor parallelism (TP) splits a single DNN layer over devices; Pipeline parallelism (PP) places different layers of a DNN model over devices (layer partitioning) and pipelines the inference to reduce devices' idling time (pipeline execution).

For DP, the small batch sizes inherent to robotic IoT applications (typically 1) hinder the mini-batch computation, rendering DP inapplicable for robotic IoT. In the data center, DP is feasible due to the large batch sizes employed (e.g., 16 images), allowing for the division of inputs into mini-batches that still contain several complete inputs (e.g., 2 images). However, in robotic IoT, real-time performance is crucial, necessitating immediate inference upon receiving inputs, which typically have smaller batch sizes (e.g., 1 image). Further splitting these inputs would result in mini-batches containing incomplete inputs (e.g., 1/4 of an image), which cannot be computed parallel to speed up inference.

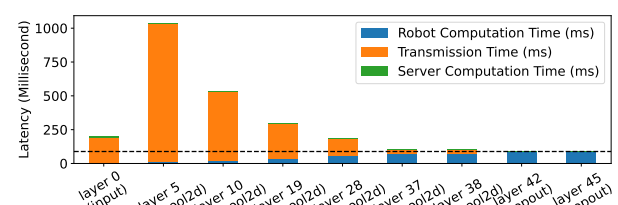
TP requires frequent synchronization among devices, leading to unacceptable communication overhead in robotic IoT.

111 By partitioning parameter tensors of a layer across GPUs,  
 112 TP allows concurrent computation on different parts of this  
 113 tensor but requires an all-reduce communication [64] to  
 114 combine computation results from different devices, which  
 115 entails significant communication overhead. Consequently,  
 116 TP is used mainly for large layers that are too large to fit in  
 117 one device in data centers and require dedicated high-speed  
 118 interconnects (e.g., 400 Gbps for NVLink [23]) even within  
 119 data centers. On the contrary, robots must prioritize seam-  
 120 less mobility and primarily depend on wireless connections,  
 121 which inherently possess limited bandwidth, as described in  
 122 Sec. 2.1, making all-reduce synchronization an unacceptable  
 123 overhead (e.g., the inference time with TP was up to 143.9X  
 124 slower than local computation in Sec.2.3.).

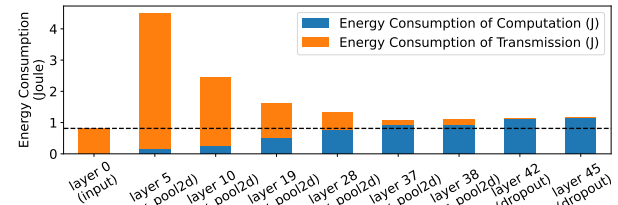
125 Consequently, existing distributed inference approaches [5,  
 126 26] in robotic IoT primarily adopt the PP paradigm and fo-  
 127 cus on layer partitioning of PP, aiming to achieve fast and  
 128 energy-efficient inference. This is because the PP paradigm  
 129 in data centers consists of layer partitioning and pipeline  
 130 execution, where the pipeline execution of PP enhances infer-  
 131 ence throughput rather than reducing the completion time of  
 132 a single inference [6], which is the most critical requirement  
 133 in robotic IoT. Based on the fact that the amounts of output  
 134 data in some intermediate layers of a DNN model are sig-  
 135 nificantly smaller than that of its raw input data [17], DNN  
 136 layer partitioning strategies constitute various trade-offs be-  
 137 tween computation and transmission, taking into account  
 138 application-specific inference speed requirements and en-  
 139 ergy consumption demands, as shown in Fig. 1.

140 However, existing methods based on PP face significant  
 141 transmission bottlenecks in robotic IoT due to the inherent  
 142 scheduling mechanism. PP paradigm on robotic IoT consists  
 143 of three sequential phases: computing earlier DNN layers on  
 144 robots, transmitting intermediate results, and completing in-  
 145 ference on the GPU server. Despite optimal layer partitioning  
 146 strategies from [5, 26], the transmission overhead becomes  
 147 a substantial bottleneck due to limited bandwidth of robotic  
 148 IoT, accounting for up to 69% of inference time in our ex-  
 149 periments. While the pipeline execution of PP can mitigate  
 150 this overhead by overlapping computation and transmis-  
 151 sion phases across multiple inference tasks, it cannot reduce  
 152 the completion time of a single inference task [6], which is  
 153 crucial for robotic applications. Furthermore, the prolonged  
 154 transmission phase not only slows down inference speed but  
 155 also consumes significantly more energy.

156 The key reason for the problem of the above methods is  
 157 that existing methods conduct layer-granulated scheduling,  
 158 whose transmission time is typically longer than the computa-  
 159 tion time due to the limited bandwidth of real-world robotic  
 160 IoT networks. As transmission time constitutes a substantial  
 161 portion of the total inference time (approximately half) in  
 162 existing methods, a novel parallel method with finer gran-  
 163 ularity that overlaps computation and transmission within  
 164 the same inference task has the potential to address this



(a) Inference Latency



(b) Energy consumption on robot

166  
 167  
 168  
 169  
 170  
 171  
 172  
 173  
 174  
 175  
 176  
 177  
 178  
 179  
 180  
 181  
 182  
 183  
 184  
 185  
 186  
 187  
 188  
 189  
 190  
 191  
 192  
 193  
 194  
 195  
 196  
 197  
 198  
 199  
 200  
 201  
 202  
 203  
 204  
 205  
 206  
 207  
 208  
 209  
 210  
 211  
 212  
 213  
 214  
 215  
 216  
 217  
 218  
 219  
 220

**Figure 1.** Existing distributed inference approaches on VGG19 [45] in our experiments, which adopt PP paradigm with various layer partitioning scheduling strategies. The X-axis of the graph represents different layer partitioning strategies, where ‘layer i’ indicates that all layers up to and including the i-th layer are computed on the robot, while the subsequent layers are processed on the GPU server.

shortcoming, achieving fast and energy-efficient inferences. Note that the robot can not enter low-power sleep mode during the transmission phase due to the need to promptly continue working upon receiving inference results, but can only enter standby mode, when chips like CPU, GPU, and memory consume non-negligible power even when not computing (e.g., 95% power consumption in our experiments). Such a parallel method would reduce the robot’s standby time without significantly increasing energy consumption during the computation phase, thereby decreasing overall energy consumption.

In this paper, we present Intra-DP (Intra-Data Parallel), a high-performance distributed inference system optimized for real-world robotic IoT networks. We discovered that operators for each DNN layer (e.g., convolution, ReLU, softmax) can be categorized into two types: local operators and global operators, depending on whether they can be computed independently without the complete input. For instance, softmax [31] requires the complete input vector to calculate the corresponding probability distribution, referring to it as a global operator, while ReLU [7] and convolution [34] can be computed with part of the input tensor (the elements in the input vector for ReLU and the blocks in the input tensor

for convolution), referring to them as local operators. Local operators need to be executed several times to complete the calculation of the whole layer; in this article, we treat each execution of the local operator as an independent local operator for easy discussion. Local operators are widely used in robotic applications, especially convolution layers in computer vision [33] and point cloud tasks [50]. The local operator granularity provides a finer granularity for Intra-DP, allowing different local operators of different layers to be computed and transmitted concurrently, enabling the overlapping of computation and transmission phases within the same inference task to achieve fast and energy-efficient inference.

The design of Intra-DP is confronted with two major challenges. The first one is how to guarantee the correctness of inference results based on local operator. We propose Local Operator Parallelism (LOP), which reduces the granularity of calculation from each layer to each local operator. LOP determines the correct input required for different local operators based on their calculation characteristics and processes at first. When a part of the local operators in a layer completes the calculation and the tensor composed of these local operators satisfies the input requirements of the local operators in the subsequent layer, the local operators in the subsequent layer can be calculated in advance, without waiting for all local operators of the current layer to be computed in LOP. For global operator layers, Intra-DP enforces a synchronization before these layers to combine the complete input for them, as TP's all-reduce communications do. In this way, Intra-DP only change the execution sequence of local operators among local operator layers and ensures the calculation correctness of local operator layers through LOP and global operator layers through synchronization. We formally prove that LOP guarantees the correctness of inference results in Sec. 4.1.

The second challenge is under LOP, how to properly schedule the computation and transmission of each local operator to achieve fast and energy-efficient inference under various hardware conditions and network bandwidths. Intra-DP places part of the local operator execution on GPU servers and transmits the corresponding part of the input tensor based on LOP, while computing the rest of the local operators with a novel Local Operator Scheduling Strategy (LOSS). LOSS formulates the problem of determining which part of the local operators should be executed on robots and which part should be executed on GPU servers as a nonlinear optimization problem (see Sec. 4.2), and schedules the computation and transmission of each local operator based on the solution obtained via the differential evolution algorithm [42].

We implemented Intra-DP in PyTorch [40] and evaluated Intra-DP on our real-world robots under two typical real-world robotic applications [33, 50] and several models common to mobile devices on a larger scale [45, 46, 48, 52, 57].

We compared Intra-DP with two SOTA pipeline parallelism methods as baselines: DSCCS [26], aimed at accelerating inference, and SPSO-GA [5], focused on optimizing energy consumption, under different real-world robotic IoT networks environments (namely indoors and outdoors). Evaluation shows that:

- Intra-DP is fast. Intra-DP reduced inference time by 80% ~98% compared to baselines under indoors and outdoors environments.
- Intra-DP is energy-efficient. Intra-DP reduced 91% ~98% energy consumption per inference compared to baselines, due to faster inference speed and no-increased power consumption against time.
- Intra-DP is robust in various robotic IoT environments. When the robotic IoT environment changed (from indoors to outdoors), Intra-DP's superior performance remained consistent.
- Intra-DP is easy to use. It took only two lines of code to apply Intra-DP to existing ML applications.

Our main contribution are LOP, a fine-grained parallel method based on local operators, and LOSS, a new scheduling strategy based on LOP optimized for distributed inference over real-world robotic IoT networks. By leveraging these contributions, Intra-DP dramatically reduces the transmission overhead in existing distributed inference on robotic IoT by overlapping the computation and transmission phases within the same inference task, achieving fast and energy-efficient distributed inference on robotic IoT. We envision that the fast and energy-efficient inference of Intra-DP will foster the deployment of diverse robotic tasks on real-world robots in the field. Intra-DP's code is released on <https://github.com/xxx/xxx>.

In the rest of this paper, we introduce the background of this paper in Sec. 2, give an overview of Intra-DP in Sec. 3, present the detailed design of Intra-DP in Sec. 4, evaluate Intra-DP in Sec. 6, and finally conclude in Sec. 7.

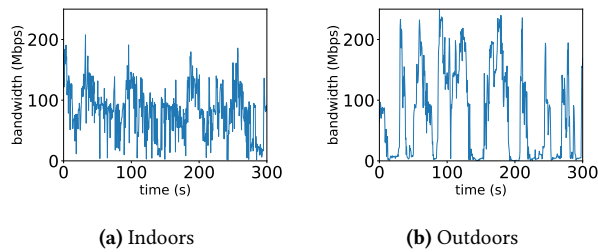
## 2 background

### 2.1 Characteristics of Robotic IoT

In real-world robotic IoT scenarios, devices often navigate and move around for tasks like search and exploration. While wireless networks provide high mobility, they also have limited bandwidth. For instance, Wi-Fi 6, the most advanced Wi-Fi technology, offers a maximum theoretical bandwidth of 1.2 Gbps for a single stream [29]. However, not only the limited hardware resources on the robot can not fully play the potential of Wi-Fi 6 [59], but also the actual available bandwidth of wireless networks is often reduced in practice due to factors such as movement of the devices [32, 39], occlusion from by physical barriers [9, 44], and preemption of the wireless channel by other devices [2, 43].

To demonstrate the instability of wireless transmission in real-world situations, we conducted a robot surveillance

331 experiment using four-wheel robots navigating around several given points at 5-40cm/s speed in our lab (indoors) and  
 332 campus garden (outdoors), with hardware and wireless net-  
 333 work settings as described in Sec. 6. We believe our setup  
 334 represents robotic IoT devices’ state-of-the-art computation  
 335 and communication capabilities. We saturated the wireless  
 336 network connection with iperf [1] and recorded the average  
 337 bandwidth capacity between these robots every 0.1s for 5  
 338 minutes.  
 339



340  
 341  
 342  
 343  
 344  
 345  
 346  
 347  
**Figure 2.** The instability of wireless transmission in robotic  
 348 IoT networks.  
 349

350 The results in Fig. 2 show average bandwidth capacities  
 351 of 93 Mbps and 73 Mbps for indoor and outdoor scenarios,  
 352 respectively. The outdoor environment exhibited higher in-  
 353 stability, with bandwidth frequently dropping to extremely  
 354 low values around 0 Mbps, due to the lack of walls to reflect  
 355 wireless signals and the presence of obstacles like trees be-  
 356 tween communicating robots, resulting in fewer received  
 357 signals compared to indoor environments.  
 358

359 In summary, robotic IoT systems’ wireless transmission  
 360 is constrained by limited bandwidth, both due to the theo-  
 361 retical upper limit of wireless transmission technologies and  
 362 the practical instability of wireless networks. Moreover, the  
 363 unstable bandwidth in robotic IoT wireless networks can  
 364 cause the transmission time to vary dramatically, sometimes  
 365 changing by hundreds of times. In our experiments, even  
 366 a relatively small model with only 0.84M parameters still  
 367 suffers from its significant transmission overhead.  
 368

## 369 2.2 Characteristics of Data Center Networks

370 Data center networks, which are used for large model in-  
 371 ference (e.g., ChatGPT [54]), are wired and typically exhibit  
 372 higher bandwidth capacity and lower fluctuation compared  
 373 to robotic IoT networks. GPU devices in data centers are  
 374 interconnected using high-speed networking technologies  
 375 such as InfiniBand [49] or PCIe [23], offering bandwidths  
 376 ranging from 40 Gbps to 500 Gbps. The primary cause of  
 377 bandwidth fluctuation in these networks is congestion on  
 378 intermediate switches, which can be mitigated through traf-  
 379 fic scheduling techniques implemented on the switches [36].  
 380 The stable and high-bandwidth nature of data center net-  
 381 works makes them well-suited for demanding tasks like  
 382

383 large model inference, in contrast to the more variable and  
 384 resource-constrained environments found in robotic IoT net-  
 385 works.  
 386

## 387 2.3 Existing distributed inference methods in the 388 data center

389 **Data parallelism.** Data parallelism [56] is a widely used  
 390 technique in distributed inference that partitions input data  
 391 across multiple devices, such as GPUs, to perform parallel  
 392 inference. Each device maintains a complete model replica  
 393 and independently processes a subset of the input data (mini-  
 394 batch), aggregating results to generate the final output. Data  
 395 parallelism enhances throughput by distributing workload  
 396 across devices, leveraging their combined computational  
 397 power.  
 398

399 However, data parallelism’s scalability is constrained by  
 400 the total batch size [35], which is particularly problematic  
 401 in robotic IoT applications where smaller batch sizes are  
 402 inherent due to the need for swift environmental responses.  
 403 In robotic applications, immediate inference upon receiving  
 404 inputs is crucial for obtaining real-time target points quickly.  
 405 For example, in our experiments, the robot constantly obtains  
 406 the latest images from the camera for inference, with a batch  
 407 size of only 1. These small batches cannot be further split  
 408 into mini-batches, a fundamental requirement for effective  
 409 data parallelism.  
 410

411 **Tensor parallelism.** Tensor parallelism [64] is a dis-  
 412 tributed inference technique that divides a model’s layer  
 413 parameters across multiple devices, each storing and com-  
 414 puting a portion of the weights. This approach requires an  
 415 all-reduce communication step after each layer to combine  
 416 results from different devices, introducing significant over-  
 417 head, especially for large DNN layers. To mitigate this, TP is  
 418 typically deployed across GPUs within the same server in  
 419 data centers, using fast intra-server GPU-to-GPU links like  
 420 NVLink [23], which is beneficial when the model is too large  
 421 for a single device.  
 422

423 In contrast to data center networks, the limited bandwidth  
 424 in robotic IoT renders the communication cost of TP prohib-  
 425 itively high, as evidenced by our evaluation of DINA [34],  
 426 a state-of-the-art TP method. Table 1 reveals that transmis-  
 427 sion time constitutes 49% to 94% of the total inference time  
 428 due to all-reduce communication for each layer, resulting  
 429 in TP’s inference time being 45.2X to 143.9X longer than  
 430 local computation. Although Table 2 indicates lower power  
 431 consumption with TP (13.4% to 67.3% less than local computa-  
 432 tion), the extended transmission times significantly increase  
 433 energy consumption per inference, ranging from 28.5X to  
 434 62.7X. Since TP significantly extends inference time, making  
 435 it impractical for real-world robotic applications, we did not  
 436 further consider TP in this paper.  
 437

438 **Pipeline parallelism.** Pipeline parallelism [18] is a dis-  
 439 tributed inference technique that partitions DNN model  
 440

Model(number of parameters)	Local computation time(s)	Environment	Transmission time (s) with TP	Inference time (s) with TP	Percentage(%) with TP
MobileNet_V3_Small(2M)	0.031( $\pm 0.004$ )	indoors outdoors	0.698( $\pm 0.135$ ) 0.901( $\pm 0.778$ )	1.400( $\pm 0.232$ ) 1.775( $\pm 1.370$ )	49.85 51.23
ResNet101(44M)	0.065( $\pm 0.005$ )	indoors outdoors	7.156( $\pm 3.348$ ) 8.470( $\pm 6.337$ )	8.106( $\pm 3.403$ ) 9.356( $\pm 6.328$ )	87.95 90.46
VGG19_BN(143M)	0.063( $\pm 0.002$ )	indoors outdoors	5.152( $\pm 4.873$ ) 5.407( $\pm 6.673$ )	5.444( $\pm 4.831$ ) 5.759( $\pm 6.635$ )	70.18 93.70

**Table 1.** Average transmission time (Second), inference time (Second), percentage that transmission time accounts for of inference time and their standard deviation ( $\pm n$ ) with TP on different models in different environments. “Local computation” refers to placing the whole layers on the robot.

Model(number of parameters)	Environment	Power consumption(W)		Energy consumption(J) per inference	
		Local	TP	Local	TP
MobileNet_V3_Small(2M)	indoors outdoors	6.05( $\pm 0.21$ ) 6.05( $\pm 0.21$ )	5.24( $\pm 0.19$ ) 5.11( $\pm 0.28$ )	0.3( $\pm 0.09$ ) 0.3( $\pm 0.09$ )	7.33( $\pm 1.21$ ) 9.08( $\pm 7.0$ )
ResNet101(44M)	indoors outdoors	11.27( $\pm 0.51$ ) 11.27( $\pm 0.51$ )	4.97( $\pm 0.16$ ) 4.9( $\pm 0.23$ )	0.93( $\pm 0.19$ ) 0.93( $\pm 0.19$ )	40.28( $\pm 16.91$ ) 45.8( $\pm 30.98$ )
VGG19_BN(143M)	indoors outdoors	14.86( $\pm 0.43$ ) 14.86( $\pm 0.43$ )	4.88( $\pm 0.29$ ) 4.87( $\pm 0.27$ )	1.19( $\pm 0.18$ ) 1.19( $\pm 0.18$ )	26.55( $\pm 23.56$ ) 28.06( $\pm 32.33$ )

**Table 2.** Power consumption against time (Watt) and energy consumption per inference (Joule) with standard deviation ( $\pm n$ ) with TP on different models in different environments. “Local” represents “Local computation”

layers across multiple devices(layer partitioning), forming an inference pipeline for concurrent processing of multiple tasks. While PP can increase throughput and resource utilization via pipeline execution, it primarily focuses on enhancing overall throughput rather than reducing single-inference latency [6], which is crucial in robotic IoT. As a result, existing distributed inference approaches [5, 26] in robotic IoT primarily adopt PP paradigm and focus on layer partitioning to achieve fast and energy-efficient inference, with two main categories based on their optimization goals: accelerating inference for diverse DNN structures [17, 21, 26, 34, 58] and optimizing robot energy consumption during inference [5, 27, 53]. Both two kinds of methods suffer from the transmission bottleneck inherent to PP’s scheduling mechanism, which can be eliminated by Intra-DP.

## 2.4 Other methods to speed up DNN Models

### Inference on Robotic IoT

**Compressed communication.** Compressed communication is crucial for efficient distributed inference in wireless networks, as it significantly reduces communication overhead through techniques such as quantization and model distillation. Quantization [8, 13, 14] is a technique that reduces the numerical precision of model weights and activations, thereby minimizing the memory footprint and

computational requirements of deep learning models. This process typically involves converting high-precision (e.g., 32-bit) floating-point values to lower-precision (e.g., 8-bit) floating-point representations, with minimal loss of model accuracy. Model distillation [15, 28, 51], on the other hand, is an approach that involves training a smaller, more efficient “student” model to mimic the behavior of a larger, more accurate “teacher” model by minimizing the difference between the student model’s output and the teacher model’s output. The distilled student model retains much of the teacher model’s accuracy while requiring significantly fewer resources. These model compression methods complement distributed inference by achieving faster inference speed through model modifications, potentially sacrificing some accuracy with smaller models, while distributed inference realizes fast inference without loss of accuracy by intelligently scheduling computation tasks across multiple devices.

**Inference Job scheduling.** Significant research efforts have been devoted to exploring inference parallelism and unleashing the potential of layer partition to accelerate DNN inference, such as inference job scheduling, aiming to accelerate multiple DNN inference tasks by optimizing their execution on various devices under different network bandwidths while considering application-specific inference speed requirements and energy consumption demands. For instance, [3,

[551] support online scheduling of offloading inference tasks  
 [552] based on the current network and resource status of mobile  
 [553] systems while meeting user-defined energy constraints. [11]  
 [554] focused on optimizing DNN inference workloads in cloud  
 [555] computing using a deep reinforcement learning based sched-  
 [556] ule for QoS-aware scheduling of heterogeneous servers, aim-  
 [557] ing to maximize inference accuracy and minimize response  
 [558] delay. While these methods focus on overall optimization in  
 [559] multi-task scenarios involving multi-robots, they do not ad-  
 [560] dress the optimization of single inference tasks and are thus  
 [561] orthogonal to distributed inference for a single inference,  
 [562] where improved distributed inference can provide faster and  
 [563] more energy-efficient inference for these scenarios.

### 3 Overview

#### 3.1 Workflow of Intra-DP

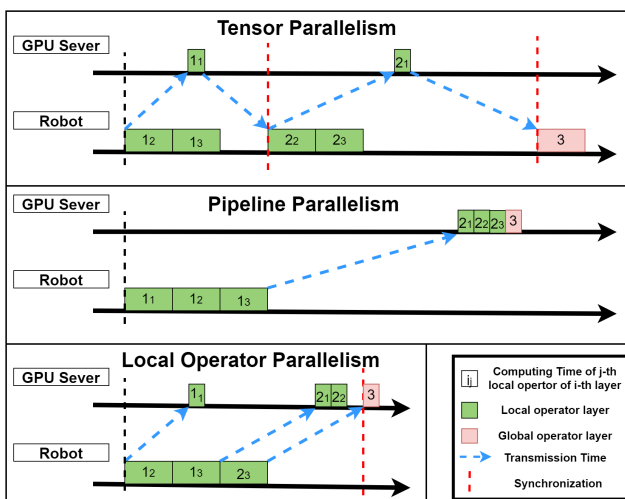


**Figure 3.** Workflow of Intra-DP. Each local operator layer have to complete the calculation of three local operators, and the same local operator in the three cases has the same computation time on robots and GPU servers, as well as the corresponding transmission time. The output tensor volume of layer 2 is larger than that of layer 1, resulting in longer transmission times for local operators in layer 2, and PP selects a layer partition strategy at layer 1 [26].

Fig. 3 presents the workflow of Intra-DP and compares it with TP and PP under robotic IoT networks with limited bandwidth, illustrating why existing methods suffer from transmission overhead and how Intra-DP solves this issue via its LOP.

While TP can place some local operator execution on the GPU server, it requires an all-reduce communication [64] to combine computation results from different devices, which entails significant communication overhead (as shown by the red dotted lines for synchronization Fig. 3). Although the layer partition algorithm [26] can be used to minimize

overall inference time, the transmission time still becomes a significant bottleneck, as illustrated by the extremely long transmission in Fig. 3.

To alleviate the transmission overhead in distributed inference, Intra-DP overlaps the computation and transmission of different local operators from different local operator layers, as shown in Fig. 3. Compared with TP, Intra-DP cancels the synchronization of the all-reduce communication for local operator layers and ensures that each local operator can get the required input in time and obtain the correct calculation results through LOP, rather than relying on all-reduce communication for local operator layers. Intra-DP maintains synchronization for global operator layers, which do not have local operators and require the complete input (the entire output tensor of the previous layer) to perform the calculation, ensuring the correctness of the global operator layers' inference. Compared with PP, Intra-DP starts transmitting some local operators and the corresponding input in advance, without waiting for all local operators in the current local operator layer to complete the calculation. In this way, Intra-DP achieves much faster inference compared with existing distributed inference methods.

Moreover, the idle time on the robot (when the robot is not computing, as shown in Fig. 3) consumes significant energy. This is because the robot cannot enter a low-power sleep mode while waiting for the final inference result from the GPU server, as it has to promptly continue working when it receives the inference results. During the standby phase (idle time), chips like CPU, GPU, and memory consume non-negligible power even when not computing, due to the static power consumption rooted in transistors' leakage current [22]. Meanwhile, we found that wireless network cards consume only 0.21 Watt for transmission during the idle time, while the robot consumes 13.35 Watt during computing. In this way, Intra-DP dramatically reduces the idle time on the robot, alleviating the energy wasted by standby mode, and increases a negligible amount of network card transmission power consumption during computing, thereby reducing the overall energy consumption for each inference.

To achieve the workflow shown in Fig. 3, the design of Intra-DP must tackle two problems: guaranteeing the correctness of inference results based on local operators and scheduling the computation and transmission of each local operator. In Sec.4.1, we will explain how Intra-DP ensures that each local operator can still obtain the correct calculation result via LOP, and in Sec.4.2, we will discuss how Intra-DP achieves fast and energy-efficient inference through its LOSS.

#### 3.2 Architecture of Intra-DP

Fig. 4 shows the architecture of Intra-DP, which adds an interceptor for each DNN layer to flexibly split the input tensor and combine the output tensor for each operator. Compared

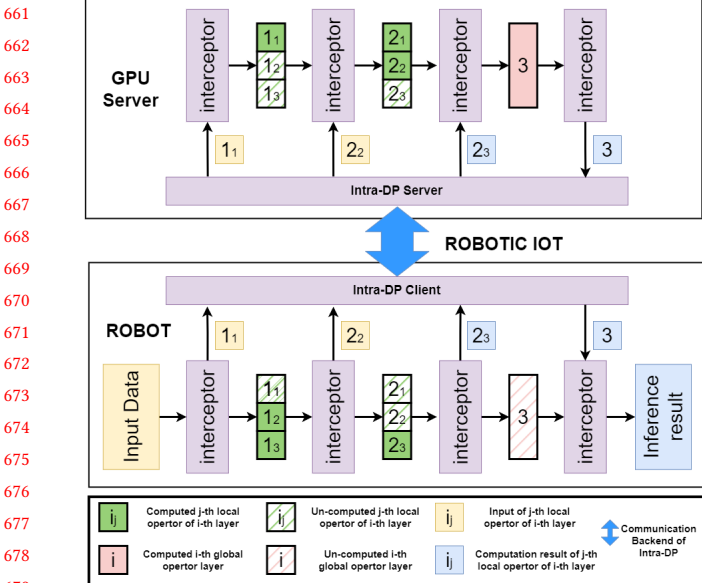


**Figure 4.** Architecture of Intra-DP. The core components of Intra-DP are highlighted in purple. Intra-DP adopts the same scheduling scheme as in Fig. 3.

with the original model inference process on the robot, Intra-DP only increases the time cost of interceptors, which is the time cost of splitting the input tensor and combining the output tensor. The time cost of splitting the input tensor is negligible because the data transfer can be completed through the backend processes of the Intra-DP client and server while the local operators assigned to be executed on the robot and GPU server continue to perform subsequent layer calculations. The time cost of combining the output tensor is mainly bound by the time when the device on the other side completes the corresponding computation and transmission, causing prolonged waiting time. Intra-DP formulates such waiting time into the nonlinear optimization problem in its LOSS, minimizing the waiting time and implementing scheduling schemes on local operators with a higher degree of parallelism. In this way, Intra-DP only increases negligible extra time on system cost and achieves faster inference via LOP and LOSS.

To address frequent fluctuations in real-world wireless networks of robotic IoT, Intra-DP generates optimal local operator scheduling strategies for the DNN model under different bandwidth conditions in advance. During inference, Intra-DP predicts the network bandwidth using mature tools [62] in the field of wireless transmission and adopts the corresponding scheduling strategy based on the predicted bandwidth. To ensure that Intra-DP can flexibly switch among various scheduling strategies, it keeps a copy of the model on the robot at the GPU server (Fig. 4), avoiding unnecessary transmission when migrating the parameters of local operators between robots and the GPU server. It is important to note

that the model inference time, typically tens or hundreds of milliseconds, is finer (smaller) than the granularity (or frequency) of bandwidth fluctuation in real-world robotic IoT networks, as shown in Fig. 2. Therefore, we assume that the network bandwidth of robotic IoT during each inference is stable, while the network bandwidth for different inferences may differ.

## 4 Detailed Design

### 4.1 Local Operator Parallelism

LOP guarantees the correctness of inference results by determining the correct input required for different local operators based on their calculation characteristics and processes. We summarize three classes of local operators common in models used on mobile devices:

- Element-wised local operator. This class of operators compute each element of the input tensor separately, requiring only the corresponding element from the input tensor to perform the calculation. They are widely used in activation functions such as ReLU [7], Sigmoid [61], SiLU [19]. However, it is important to note that some activation functions, like softmax [31], require all elements for computation and are not considered local operators, but global operators.
- Block-wised local operator. This class of operators require a block at the corresponding position in the input tensor and are widely used in layers associated with convolution, such as convolution [34], max-pool [47]. The size of the input blocks is determined by the parameters set by the corresponding layer [41], including the size of the convolution kernel, padding, and dilation.
- Row-wised local operator. This class of operators requires rows of the input tensor and are widely used in layers associated with matrix operations, such as addition [63] and multiplication [12]. The rows required for computation, ensuring that the correct input is obtained for each local operator to perform its respective calculation, are determined by the matrix calculation principles as following:

$$\begin{pmatrix} a_1 \\ \vdots \\ a_m \end{pmatrix} \times (b_1 \quad \cdots \quad b_n) = \begin{pmatrix} c_{11} & \cdots & c_{1n} \\ \vdots & \ddots & \vdots \\ c_{m1} & \cdots & c_{mn} \end{pmatrix}$$

Row-wised local operators split the input matrix and keep a copy of the layer parameter matrix on different devices, reducing transmission volume and avoiding the synchronization needed to combine calculation results from different devices. This is in contrast to TP, which splits the layer parameter matrix and transfers a copy of the input matrix to different devices. The calculation result of row  $a_1$  is  $(c_{11} \cdots c_{1n})$ , which is also a row and can be directly computed by the next

771 matrix operation layer. And LOP treats matrices with  
 772 only one row as global operators.

773 After obtaining the required input for each local operator  
 774 and the corresponding input position in the previous layer  
 775 through the above analysis, LOP determines which local  
 776 operators need to be computed in the previous layer to obtain  
 777 the input for the current local operator. This establishes  
 778 the dependency between local operators, which should be  
 779 considered when scheduling local operators as LOSS. And  
 780 we leave the support for additional types of local operators  
 781 as future work.

## 783 4.2 Local Operator Scheduling Strategy

784 §

## 786 4.3 Algorithms of Intra-DP

---

### Algorithm 1: Local\_Operator\_Scheduling\_Strategy

---

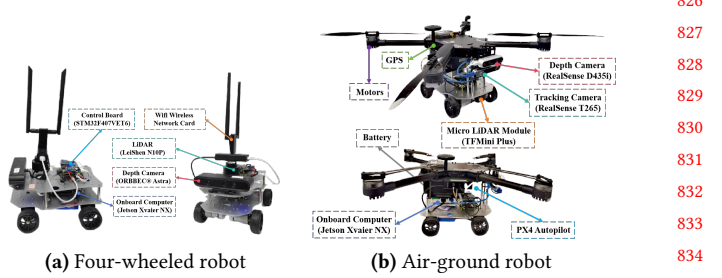
789 **Input:** Cuda kernel function called by the corresponding  
 790 operator *func* and the required parameters *args*  
 791 **Output:** The execution result *ret*  
 792 **Data:** inference operator sequence *IOS* = 0  
 793 1 **if** *IOS.empty()* **then**  
 794     // recorder  
 795     *SendRPCtoServer(func, args)*  
 796     *IOS = DataDependencySearch(func, args)*  
 797     *ret = GetRPCExecutionResult()*  
 798     *RecordReturn(ret)*  
 799 2 **end**  
 800 3 **else**  
 801     // replayer on robot  
 802     **if** *func == IOS.start()["func"]* **then**  
 803         *ret = StartRRTO(args, IOS)*  
 804         // start a new inference  
 805     **end**  
 806     **else if** *func == IOS.end()["func"]* **then**  
 807         *ret = WaitingForRRTO()*  
 808         // Waiting for the final computation result  
 809     **end**  
 810     **else**  
 811         *ret = IOS.find(func)["ret"]*  
 812     **end**  
 813 17 **end**  
 814 18 **return** *ret*

---

## 819 5 Implementation

## 820 6 Evaluation

822 **Testbed.** The evaluation was conducted on a custom four-  
 823 wheeled robot (Fig 5a), and a custom air-ground robot(Fig 5b).  
 824 They are equipped with a Jetson Xavier NX [37] 8G onboard  
 825



834 **Figure 5.** The detailed composition of the robot platforms

	inference	transmission	standby
Power (W)	13.35	4.25	4.04

835 **Table 3.** Power consumption (Watt) of our robot in different  
 836 states.

843 computer that is capable of AI model inference with local  
 844 computation resources. The system runs Ubuntu 20.04 with  
 845 ROS Noetic and a dual-band USB network card (MediaTek  
 846 MT76x2U) for wireless connectivity. The Jetson Xavier NX  
 847 interfaces with a Leishen N10P LiDAR, ORBBEC Astra depth  
 848 camera, and an STM32F407VET6 controller via USB serial  
 849 ports. Both LiDAR and depth cameras facilitate environmental  
 850 perception, enabling autonomous navigation, obstacle  
 851 avoidance, and SLAM mapping. The GPU server accepting  
 852 offloaded computation tasks from the robot is a PC equipped  
 853 with an Intel(R) i5 12400f CPU @ 4.40GHz and an NVIDIA  
 854 GeForce GTX 2080 Ti 11GB GPU, connected to our robot  
 855 via WiFi 6 over 80MHz channel at 5GHz frequency in our  
 856 experiments.

857 Tab. 3 presents the overall on-board energy consumption  
 858 (excluding motor energy consumption for robot movement)  
 859 of the robot in various states: inference (model inference  
 860 with full GPU utilization, including CPU and GPU energy  
 861 consumption), transmission (communication with the GPU  
 862 server, including wireless network card energy consump-  
 863 tion), and standby (robot has no tasks to execute). Notice  
 864 that different models, due to varying numbers of parameters,  
 865 exhibit distinct GPU utilization rates and power consump-  
 866 tion during inference.

867 **Experiment Environments.** We evaluated two real-world  
 868 environments: indoors (robots move in our laboratory with  
 869 desks and separators interfering with wireless signals) and  
 870 outdoors (robots move in our campus garden with trees and  
 871 bushes interfering with wireless signals, resulting in lower  
 872 bandwidth). The corresponding bandwidths between the  
 873 robot and the GPU server in indoors and outdoors scenarios  
 874 are shown in Fig. 2.

875 **Workload.** We evaluated two typical real-world robotic  
 876 applications on our testbed: Kapao, a real-time people-tracking

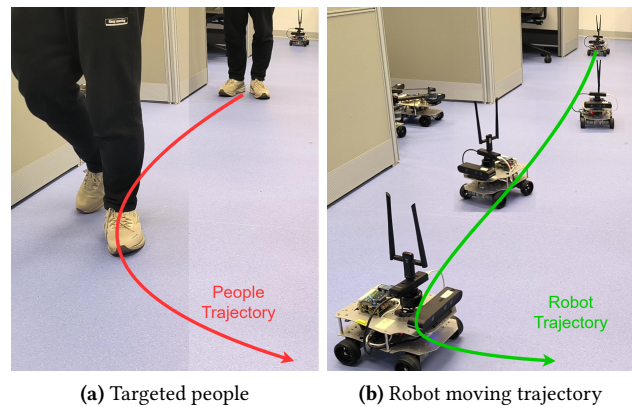


**Figure 6.** A real-time people-tracking robotic application on our robot based on a well-known human pose estimation ML model, Kapao [33].

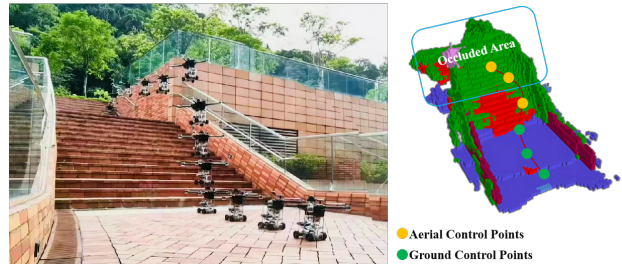


**Figure 7.** By predicting occlusions in advance, AGRNav [50] gains an accurate perception of the environment and avoids collisions, resulting in efficient and energy-saving paths.

application on our four-wheeled robot (Fig 6), and AGRNav, an autonomous navigation application on our air-ground robot (Fig 7). These applications feature different model input and output size patterns: Kapao takes RGB images as input and outputs key points of small data volume. In contrast, AGRNav takes point clouds as input and outputs predicted point clouds and semantics of similar data volume as input, implying that AGRNav needs to transmit more data during offloading. And we have verified several models common to mobile devices on a larger scale to further corroborate our observations and findings: MobileNet [46], ResNet [48], VGGNet [45], ConvNeXt [52], RegNet [57].

**Baselines.** We selected two SOTA pipeline parallelism methods as baselines: DSCCS [26], aimed at accelerating inference, and SPSO-GA [5], focused on optimizing energy consumption. We set SPSO-GA’s deadline constraints to 1 Hz, the minimum frequency required for robot movement control. Given our primary focus on inference time and energy consumption per inference, we disabled pipeline execution to concentrate solely on assessing the performance of various layer partitioning methods.

## 6.1 Inference Time

**Kapao.** From the results in the upper part of Tab. 4, both SPSO-GA and DSCCS reduced Kapao’s inference time by 39.69% and 56.92% indoors and 28.67% and 47.46% outdoors, with DSCCS achieving 28.57% (indoors) and 26.34% (outdoors) lower inference time than SPSO-GA. While both systems significantly reduced inference time via offloading, transmission time accounts for 49.69% to 69.46% of the whole inference time, indicating that even with SOTA layer partitioning, the transmission bottleneck inherent to PP’s scheduling mechanism cannot be mitigated. The difference between DSCCS and SPSO-GA can be attributed to their optimization goals: DSCCS minimizes inference latency, while SPSO-GA minimizes power consumption under deadline constraints.

**AGRNav.** The performance gain of the two offloading systems varied for AGRNav, as shown in the lower part of Tab. 4. DSCCS still reduced inference time by 18.34% and 12.43% in indoors and outdoors. However, SPSO-GA achieved similar inference time (3.65% and 3.06% reduction) as local computation both indoors and outdoors. We will explain and analyze this phenomenon in Sec.6.2.

Notice that the large standard deviation in transmission time in outdoors in both offloading systems indicates that bandwidth fluctuated more frequently and more fiercely outdoors compared with indoors, which complies with Fig. 2. Additionally, the lower average bandwidth for outdoors scenarios (see Sec.2.1) results in increased transmission and inference times relative to indoor scenarios.

## 6.2 Breakdown

Both SPSO-GA and DSCCS automatically adapt to available bandwidth, transitioning to edge computation (placing all DNN layers on the GPU server) when bandwidth is sufficient, and to local computation (placing all DNN layers on robots) when bandwidth is low. To better understand how their layer partitioning scheduling varies with different network conditions and models, we recorded and analyzed the Categories and percentages of various layer partitioning schedules under different baselines and environments, as detailed in Fig. 8.

Local computation and edge computation are special cases of layer partitioning, with the bandwidth conditions required for each model to reach these cases varying based on the model structure and partitioning method used. Analyzing Fig. 8a and Fig. 8b, both SPSO-GA and DSCCS tend to allocate more layers on the robot for AGRNav. When comparing indoor and outdoor scenarios in Fig. 8, it is evident that higher bandwidth leads to more layers being scheduled on GPU server. Additionally, when comparing SPSO-GA and DSCCS in Fig. 8, DSCCS, which focuses on optimizing energy consumption, tends to place fewer layers on the robot to reduce computation energy consumption.

Model(number of parameters)	Local computation time (s)	Environment	Transmission time (s)			Inference time (s)		
			DSCCS	SPSO-GA	Intra-DP	DSCCS	SPSO-GA	Intra-DP
kapao(77M)	0.78( $\pm 0.23$ )	indoors	0.228( $\pm 0.176$ )	0.235( $\pm 0.164$ )	0.259( $\pm 0.181$ )	0.343( $\pm 0.192$ )	0.311( $\pm 0.168$ )	0.264( $\pm 0.148$ )
		outdoors	0.087( $\pm 0.178$ )	0.35( $\pm 1.045$ )	0.385( $\pm 1.15$ )	0.696( $\pm 0.125$ )	0.434( $\pm 1.046$ )	0.369( $\pm 0.49$ )
agrnav(0M)	1.12( $\pm 0.11$ )	indoors	0.266( $\pm 0.166$ )	0.239( $\pm 0.149$ )	0.263( $\pm 0.164$ )	0.433( $\pm 0.134$ )	0.427( $\pm 0.12$ )	0.365( $\pm 0.50$ )
		outdoors	0.263( $\pm 0.843$ )	0.218( $\pm 0.796$ )	0.24( $\pm 0.875$ )	0.512( $\pm 0.779$ )	0.536( $\pm 0.72$ )	0.456( $\pm 0.52$ )

**Table 4.** Average transmission time (Second), inference time (Second), percentage that transmission time accounts for of inference time and their standard deviation ( $\pm n$ ) of Kapao and AGRNav with different pipeline parallelism offloading systems and different environments. “Local computation” refers to placing the whole layers on the robot.

Model(number of parameters)	Environment	Power consumption(W)			Energy consumption(J) per inference			
		Local	DSCCS	SPSO-GA	Intra-DP	Local	DSCCS	SPSO-GA
kapao(77M)	indoors	15.04( $\pm 0.64$ )	7.03( $\pm 3.57$ )	5.92( $\pm 2.18$ )	5.03( $\pm 1.87$ )	15.03( $\pm 0.63$ )	2.41( $\pm 1.35$ )	1.84( $\pm 1.0$ )
	outdoors	15.04( $\pm 0.64$ )	14.15( $\pm 1.71$ )	5.89( $\pm 2.3$ )	5.02( $\pm 1.97$ )	1.56( $\pm 0.85$ )	9.85( $\pm 1.77$ )	2.56( $\pm 6.17$ )
agrnav(0.84M)	indoors	10.26( $\pm 1.58$ )	6.6( $\pm 1.95$ )	6.74( $\pm 2.03$ )	5.74( $\pm 1.78$ )	10.82( $\pm 1.44$ )	2.86( $\pm 0.88$ )	2.88( $\pm 0.81$ )
	outdoors	10.26( $\pm 1.58$ )	7.36( $\pm 2.34$ )	7.91( $\pm 2.45$ )	6.71( $\pm 2.1$ )	10.82( $\pm 1.44$ )	3.77( $\pm 5.74$ )	4.25( $\pm 5.7$ )

**Table 5.** The power consumption against time (Watt) and energy consumption per inference (Joule) with standard deviation ( $\pm n$ ) of Kapao and AGRNav at different baselines and environments. “Local” represents “Local computation”

In summary, the conditions under which layer partitioning schemes make these special cases are influenced by multiple factors: model structure, and the trade-offs between inference delay and energy consumption. And the higher the bandwidth, the more layers are scheduled to be placed on GPU server.

### 6.3 Energy Consumption

**Kapao.** From the results in the upper part of Tab. 5, DSCCS consumed 3.38% and 2.02% more power per second than SPSO-GA indoors and outdoors due to more layers placed on robots shown in Fig. 8a. However, SPSO-GA consumed 58.54% and 49.74% more energy overall to process a frame than DSCCS because it only aims at minimizing the power consumption against time at the cost of possibly prolonged inference time.

**AGRNav.** From the results in the lower part of Tab. 5, DSCCS consumed 61.21% and 22.92% more energy per second than SPSO-GA indoors and outdoors ( Tab. 5), while DSCCS consumed 34.15% and 5.43% more energy to process a frame than SPSO-GA. SPSO-GA’s advantages in power consumption against time shrinks in energy consumption per inference due to prolonged inference time.

### 6.4 Validation on a larger range of models

We evaluated PP across a broad range of models with varying parameter counts (from 0.84M to 644M, as detailed in Tab. 6 and Tab. 7), which are commonly used in mobile devices. Our findings confirm that transmission time constitutes a significant portion of the total inference time in robotic IoT

when using PP. The inherent transmission overhead of PP’s scheduling mechanism significantly wastes both inference time and energy.

## 6.5 Lessons learned

**Global optimal solution.** for nonlinear optimization problem

**Wireless bandwidth prediction.**

**Distributed inference system for multiple robots.**

## 7 Conclusion

In this paper, we explored the problems that hinder the application of existing parallel methods for distributed inference on robotic IoT, including the failure of data parallelism due to small batch sizes, the unacceptable communication overhead of tensor parallelism caused by all-reduce communication, and the significant transmission bottlenecks inherent to pipeline parallelism’s scheduling mechanism. By raising awareness of these issues, we aim to stimulate research efforts towards developing novel parallel methods that address these problems. We envision that fast and energy-efficient inference will foster the deployment of diverse robotic tasks on real-world robots in the field.

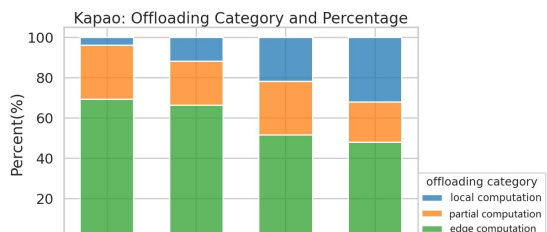
## References

- [1] [n. d.]. iPerf - Download iPerf3 and original iPerf pre-compiled binaries. <https://iperf.fr/iperf-download.php>
- [2] Toni Adame, Marc Carrascosa-Zamacois, and Boris Bellalta. 2021. Time-sensitive networking in IEEE 802.11 be: On the way to low-latency WiFi 7. *Sensors* 21, 15 (2021), 4954.

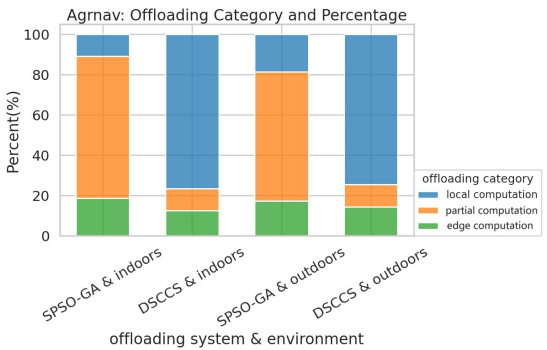
	Model(number of parameters)	Local computation time (s)	Environment	Transmission time (s)		Inference time (s)		Percentage(%)
				SPSO-GA	DSCCS	SPSO-GA	DSCCS	SPSO-GA   DSCCS
1101 1102 1103 1104 1105 1106 1107 1108 1109 1110 1111 1112 1113 1114 1115	MobileNet_V3_Small (2M)	0.033( $\pm 0.019$ )	indoors	0.035( $\pm 0.019$ )	0.016( $\pm 0.005$ )	0.044( $\pm 0.020$ )	0.031( $\pm 0.008$ )	79.79
			outdoors	0.035( $\pm 0.044$ )	0.017( $\pm 0.005$ )	0.047( $\pm 0.037$ )	0.033( $\pm 0.018$ )	50.04
1116 1117 1118 1119 1120	RegNet_X_3_2GF (15M)	0.060( $\pm 0.022$ )	indoors	0.049( $\pm 0.026$ )	0.033( $\pm 0.011$ )	0.065( $\pm 0.028$ )	0.049( $\pm 0.016$ )	76.25
			outdoors	0.049( $\pm 0.055$ )	0.032( $\pm 0.032$ )	0.069( $\pm 0.050$ )	0.051( $\pm 0.030$ )	53.23
1121 1122 1123 1124 1125 1126 1127 1128 1129 1130 1131 1132 1133 1134 1135	ResNet101 (44M)	0.060( $\pm 0.023$ )	indoors	0.054( $\pm 0.451$ )	0.033( $\pm 0.010$ )	0.072( $\pm 0.453$ )	0.050( $\pm 0.016$ )	75.64
			outdoors	0.052( $\pm 0.064$ )	0.033( $\pm 0.036$ )	0.077( $\pm 0.059$ )	0.054( $\pm 0.034$ )	51.54
1136 1137 1138 1139 1140 1141 1142 1143 1144 1145 1146 1147 1148 1149 1150 1151 1152 1153 1154 1155	ConvNeXt_Base (88M)	0.047( $\pm 0.004$ )	indoors	0.033( $\pm 0.018$ )	0.020( $\pm 0.006$ )	0.044( $\pm 0.019$ )	0.032( $\pm 0.009$ )	75.39
			outdoors	0.032( $\pm 0.038$ )	0.020( $\pm 0.022$ )	0.045( $\pm 0.033$ )	0.034( $\pm 0.019$ )	52.82
1156 1157 1158 1159 1160 1161 1162 1163 1164 1165 1166 1167 1168 1169 1170	ConvNeXt_Large (197M)	0.051( $\pm 0.005$ )	indoors	0.033( $\pm 0.017$ )	0.023( $\pm 0.008$ )	0.046( $\pm 0.019$ )	0.035( $\pm 0.013$ )	72.96
			outdoors	0.032( $\pm 0.038$ )	0.023( $\pm 0.024$ )	0.054( $\pm 0.040$ )	0.041( $\pm 0.028$ )	48.94
1171 1172 1173 1174 1175	RegNet_Y_128GF (644M)	0.139( $\pm 0.016$ )	indoors	0.076( $\pm 0.289$ )	0.041( $\pm 0.024$ )	0.305( $\pm 0.382$ )	0.100( $\pm 0.035$ )	23.58
			outdoors	0.171( $\pm 0.602$ )	0.016( $\pm 0.055$ )	0.432( $\pm 0.615$ )	0.117( $\pm 0.242$ )	32.39

**Table 6.** Average transmission time (Second), inference time (Second), percentage that transmission time accounts for of inference time and their standard deviation ( $\pm n$ ) of common AI models in different environments with different offloading systems. “Local computation” refers to placing the whole layers on the robot.

1121 1122 1123 1124 1125 1126 1127 1128 1129 1130 1131 1132 1133 1134 1135	Model(number of parameters)	Environment	Power consumption(W)			Energy consumption(J) per inference		
			Local	SPSO-GA	DSCCS	Local	SPSO-GA	DSCCS
1136 1137 1138 1139 1140 1141 1142 1143 1144 1145 1146 1147 1148 1149 1150 1151 1152 1153 1154 1155	MobileNet_V3_Small (2M)	indoors	6.131( $\pm 0.061$ )	5.448( $\pm 0.168$ )	5.658( $\pm 0.085$ )	0.202( $\pm 0.002$ )	0.241( $\pm 0.107$ )	0.174( $\pm 0.046$ )
		outdoors	6.131( $\pm 0.061$ )	5.567( $\pm 0.273$ )	5.557( $\pm 0.186$ )	0.202( $\pm 0.002$ )	0.260( $\pm 0.204$ )	0.185( $\pm 0.099$ )
1156 1157 1158 1159 1160 1161 1162 1163 1164 1165 1166 1167 1168 1169 1170	RegNet_X_3_2GF (15M)	indoors	8.208( $\pm 0.140$ )	5.490( $\pm 0.178$ )	5.714( $\pm 0.342$ )	0.492( $\pm 0.008$ )	0.356( $\pm 0.156$ )	0.278( $\pm 0.091$ )
		outdoors	8.208( $\pm 0.140$ )	5.878( $\pm 0.659$ )	6.041( $\pm 0.624$ )	0.492( $\pm 0.008$ )	0.406( $\pm 0.295$ )	0.311( $\pm 0.184$ )
1171 1172 1173 1174 1175	ResNet101 (44M)	indoors	11.851( $\pm 0.404$ )	5.457( $\pm 0.240$ )	5.953( $\pm 0.789$ )	0.711( $\pm 0.024$ )	0.390( $\pm 2.471$ )	0.298( $\pm 0.094$ )
		outdoors	11.851( $\pm 0.404$ )	6.179( $\pm 1.083$ )	6.431( $\pm 1.060$ )	0.711( $\pm 0.024$ )	0.478( $\pm 0.364$ )	0.349( $\pm 0.216$ )
1176 1177 1178 1179 1180 1181 1182 1183 1184 1185 1186 1187 1188 1189 1190	ConvNeXt_Base (88M)	indoors	15.335( $\pm 0.273$ )	5.507( $\pm 0.358$ )	7.713( $\pm 2.613$ )	0.721( $\pm 0.013$ )	0.241( $\pm 0.103$ )	0.250( $\pm 0.069$ )
		outdoors	15.335( $\pm 0.273$ )	7.638( $\pm 3.297$ )	9.148( $\pm 3.338$ )	0.721( $\pm 0.013$ )	0.346( $\pm 0.254$ )	0.307( $\pm 0.171$ )
1191 1192 1193 1194 1195 1196 1197 1198 1199 1200 1201 1202 1203 1204 1205 1206 1207 1208 1209	ConvNeXt_Large (197M)	indoors	15.403( $\pm 0.082$ )	5.518( $\pm 0.638$ )	6.604( $\pm 2.860$ )	0.786( $\pm 0.004$ )	0.251( $\pm 0.104$ )	0.230( $\pm 0.088$ )
		outdoors	15.403( $\pm 0.082$ )	8.400( $\pm 4.345$ )	8.895( $\pm 4.505$ )	0.786( $\pm 0.004$ )	0.452( $\pm 0.339$ )	0.366( $\pm 0.248$ )
1210 1211 1212 1213 1214 1215 1216 1217 1218 1219 1220 1221 1222 1223 1224 1225 1226 1227 1228 1229 1230 1231 1232 1233 1234 1235 1236 1237 1238 1239 1240 1241 1242 1243 1244 1245 1246 1247 1248 1249 1250 1251 1252 1253 1254 1255 1256 1257 1258 1259 1260 1261 1262 1263 1264 1265 1266 1267 1268 1269 1270 1271 1272 1273 1274 1275 1276 1277 1278 1279 1280 1281 1282 1283 1284 1285 1286 1287 1288 1289 1290 1291 1292 1293 1294 1295 1296 1297 1298 1299 1300 1301 1302 1303 1304 1305 1306 1307 1308 1309 1310 1311 1312 1313 1314 1315 1316 1317 1318 1319 1320 1321 1322 1323 1324 1325 1326 1327 1328 1329 1330 1331 1332 1333 1334 1335 1336 1337 1338 1339 1340 1341 1342 1343 1344 1345 1346 1347 1348 1349 1350 1351 1352 1353 1354 1355 1356 1357 1358 1359 1360 1361 1362 1363 1364 1365 1366 1367 1368 1369 1370 1371 1372 1373 1374 1375 1376 1377 1378 1379 1380 1381 1382 1383 1384 1385 1386 1387 1388 1389 1390 1391 1392 1393 1394 1395 1396 1397 1398 1399 1400 1401 1402 1403 1404 1405 1406 1407 1408 1409 1410 1411 1412 1413 1414 1415 1416 1417 1418 1419 1420 1421 1422 1423 1424 1425 1426 1427 1428 1429 1430 1431 1432 1433 1434 1435 1436 1437 1438 1439 1440 1441 1442 1443 1444 1445 1446 1447 1448 1449 1450 1451 1452 1453 1454 1455 1456 1457 1458 1459 1460 1461 1462 1463 1464 1465 1466 1467 1468 1469 1470 1471 1472 1473 1474 1475 1476 1477 1478 1479 1480 1481 1482 1483 1484 1485 1486 1487 1488 1489 1490 1491 1492 1493 1494 1495 1496 1497 1498 1499 1500 1501 1502 1503 1504 1505 1506 1507 1508 1509 1510 1511 1512 1513 1514 1515 1516 1517 1518 1519 1520 1521 1522 1523 1524 1525 1526 1527 1528 1529 1530 1531 1532 1533 1534 1535 1536 1537 1538 1539 1540 1541 1542 1543 1544 1545 1546 1547 1548 1549 1550 1551 1552 1553 1554 1555 1556 1557 1558 1559 1560 1561 1562 1563 1564 1565 1566 1567 1568 1569 1570 1571 1572 1573 1574 1575 1576 1577 1578 1579 1580 1581 1582 1583 1584 1585 1586 1587 1588 1589 1590 1591 1592 1593 1594 1595 1596 1597 1598 1599 1600 1601 1602 1603 1604 1605 1606 1607 1608 1609 1610 1611 1612 1613 1614 1615 1616 1617 1618 1619 1620 1621 1622 1623 1624 1625 1626 1627 1628 1629 1630 1631 1632 1633 1634 1635 1636 1637 1638 1639 1640 1641 1642 1643 1644 1645 1646 1647 1648 1649 1650 1651 1652 1653 1654 1655 1656 1657 1658 1659 1660 1661 1662 1663 1664 1665 1666 1667 1668 1669 1670 1671 1672 1673 1674 1675 1676 1677 1678 1679 1680 1681 1682 1683 1684 1685 1686 1687 1688 1689 1690 1691 1692 1693 1694 1695 1696 1697 1698 1699 1700 1701 1702 1703 1704 1705 1706 1707 1708 1709 17010 17011 17012 17013 17014 17015 17016 17017 17018 17019 17020 17021 17022 17023 17024 17025 17026 17027 17028 17029 17030 17031 17032 17033 17034 17035 17036 17037 17038 17039 17040 17041 17042 17043 17044 17045 17046 17047 17048 17049 17050 17051 17052 17053 17054 17055 17056 17057 17058 17059 17060 17061 17062 17063 17064 17065 17066 17067 17068 17069 17070 17071 17072 17073 17074 17075 17076 17077 17078 17079 17080 17081 17082 17083 17084 17085 17086 17087 17088 17089 17090 17091 17092 17093 17094 17095 17096 17097 17098 17099 170100 170101 170102 170103 170104 170105 170106 170107 170108 170109 170110 170111 170112 170113 170114 170115 170116 170117 170118 170119 170120 170121 170122 170123 170124 170125 170126 170127 170128 170129 170130 170131 170132 170133 170134 170135 170136 170137 170138 170139 170140 170141 170142 170143 170144 170145 170146 170147 170148 170149 170150 170151 170152 170153 170154 170155 170156 170157 170158 170159 170160 170161 170162 170163 170164 170165 170166 170167 170168 170169 170170 170171 170172 170173 170174 170175 170176 170177 170178 170179 170180 170181 170182 170183 170184 170185 170186 170187 170188 170189 170190 170191 170192 170193 170194 170195 170196 170197 170198 170199 170200 170201 170202 170203 170204 170205 170206 170207 170208 170209 170210 170211 170212 170213 170214 170215 170216 170217 170218 170219 170220 170221 170222 170223 170224 170225 170226 170227 170228 170229 170230 170231 170232 170233 170234 170235 170236 170237 170238 170239 170240 170241 170242 170243 170244 170245 170246 170247 170248 170249 170250 170251 170252 170253 170254 170255 170256 170257 170258 170259 170260 170261 170262 170263 170264 170265 170266 170267 170268 170269 170270 170271 170272 170273 170274 170275 170276 170277 170278 170279 170280 170281 170282 170283 170284 170285 170286 170287 170288 170289 170290 170291 170292 170293 170294 170295 170296 170297 170298 170299 170300 170301 170302 170303 170304 170305 170306 170307 170308 170309 170310 170311 170312 170313 170314 170315 170316 170317 170318<br								



(a) Categories and percentage of various scheduling for Kapao



(b) Categories and percentage of various scheduling for AGRNav

**Figure 8.** The layer partitioning scheduling under different baselines and environments. “Local computation” refers to placing the whole layers on the robot when the bandwidth is too low, “edge computation” means placing the whole layers on GPU server when the bandwidth is sufficient, and “partial computation” means placing part of the layers on the robot and part on GPU server.

- [12] Kayvon Fatahalian, Jeremy Sugerman, and Pat Hanrahan. 2004. Understanding the efficiency of GPU algorithms for matrix-matrix multiplication. In *Proceedings of the ACM SIGGRAPH/EUROGRAPHICS conference on Graphics hardware*. 133–137.
- [13] Stefan Gheorghe and Mihai Ivanovici. 2021. Model-based weight quantization for convolutional neural network compression. In *2021 16th International Conference on Engineering of Modern Electric Systems (EMES)*. IEEE, 1–4.
- [14] Cheng Gong, Yao Chen, Ye Lu, Tao Li, Cong Hao, and Deming Chen. 2020. VecQ: Minimal loss DNN model compression with vectorized weight quantization. *IEEE Trans. Comput.* 70, 5 (2020), 696–710.
- [15] Jianping Gou, Baosheng Yu, Stephen J Maybank, and Dacheng Tao. 2021. Knowledge distillation: A survey. *International Journal of Computer Vision* 129, 6 (2021), 1789–1819.
- [16] Vinayak Honkote, Dileep Kurian, Sriram Muthukumar, Dibyendu Ghosh, Satish Yada, Kartik Jain, Bradley Jackson, Ilya Klotchkov, Mallikarjuna Rao Nimmagadda, Shreela Dattawadkar, et al. 2019. 2.4 a distributed autonomous and collaborative multi-robot system featuring a low-power robot soc in 22nm cmos for integrated battery-powered minibots. In *2019 IEEE International Solid-State Circuits Conference-(ISSCC)*. IEEE, 48–50.

- [17] Chuang Hu, Wei Bao, Dan Wang, and Fengming Liu. 2019. Dynamic adaptive DNN surgery for inference acceleration on the edge. In *IEEE INFOCOM 2019-IEEE Conference on Computer Communications*. IEEE, 1423–1431.
- [18] Yang Hu, Connor Imes, Xuanang Zhao, Souvik Kundu, Peter A Beerel, Stephen P Crago, and John Paul Walters. 2022. Pipeedge: Pipeline parallelism for large-scale model inference on heterogeneous edge devices. In *2022 25th Euromicro Conference on Digital System Design (DSD)*. IEEE, 298–307.
- [19] Glenn Jocher, Alex Stoken, Jirka Borovec, Liu Changyu, Adam Hogan, Ayush Chaurasia, Laurentiu Diaconu, Francisco Ingham, Adrien Colmagro, Hu Ye, et al. 2021. ultralytics/yolov5: v4. 0-nm. SiLU () activations, Weights & Biases logging, PyTorch Hub integration. *Zenodo* (2021).
- [20] KJ Joseph, Salman Khan, Fahad Shahbaz Khan, and Vineeth N Balasubramanian. 2021. Towards Open World Object Detection. In *Proceedings of the IEEE/CVF Conference on Computer Vision and Pattern Recognition (CVPR)*. 5830–5840.
- [21] Yiping Kang, Johann Hauswald, Cao Gao, Austin Rovinski, Trevor Mudge, Jason Mars, and Lingjia Tang. 2017. Neurosurgeon: Collaborative intelligence between the cloud and mobile edge. *ACM SIGARCH Computer Architecture News* 45, 1 (2017), 615–629.
- [22] Nam Sung Kim, Todd Austin, David Baauw, Trevor Mudge, Krisztán Flautner, Jie S Hu, Mary Jane Irwin, Mahmut Kandemir, and Vijaykrishnan Narayanan. 2003. Leakage current: Moore’s law meets static power. *computer* 36, 12 (2003), 68–75.
- [23] Ang Li, Shuaiwen Leon Song, Jieyang Chen, Jiajia Li, Xu Liu, Nathan R Tallent, and Kevin J Barker. 2019. Evaluating modern gpu interconnect: Pcie, nvlink, nv-sli, nvswitch and gpudirect. *IEEE Transactions on Parallel and Distributed Systems* 31, 1 (2019), 94–110.
- [24] Qingbiao Li, Fernando Gama, Alejandro Ribeiro, and Amanda Prorok. 2020. Graph neural networks for decentralized multi-robot path planning. In *2020 IEEE/RSJ International Conference on Intelligent Robots and Systems (IROS)*. IEEE, 11785–11792.
- [25] Yiming Li, Zhiding Yu, Christopher Choy, Chaowei Xiao, Jose M Alvarez, Sanja Fidler, Chen Feng, and Anima Anandkumar. 2023. Voxformer: Sparse voxel transformer for camera-based 3d semantic scene completion. In *Proceedings of the IEEE/CVF Conference on Computer Vision and Pattern Recognition*. 9087–9098.
- [26] Huanghuang Liang, Qianlong Sang, Chuang Hu, Dazhao Cheng, Xiaobo Zhou, Dan Wang, Wei Bao, and Yu Wang. 2023. DNN surgery: Accelerating DNN inference on the edge through layer partitioning. *IEEE transactions on Cloud Computing* (2023).
- [27] Bing Lin, Yiniao Huang, Jianshan Zhang, Junqin Hu, Xing Chen, and Jun Li. 2019. Cost-driven off-loading for DNN-based applications over cloud, edge, and end devices. *IEEE Transactions on Industrial Informatics* 16, 8 (2019), 5456–5466.
- [28] Tao Lin, Lingjing Kong, Sebastian U Stich, and Martin Jaggi. 2020. Ensemble distillation for robust model fusion in federated learning. *Advances in Neural Information Processing Systems* 33 (2020), 2351–2363.
- [29] Ruofeng Liu and Nakjung Choi. 2023. A First Look at Wi-Fi 6 in Action: Throughput, Latency, Energy Efficiency, and Security. *Proceedings of the ACM on Measurement and Analysis of Computing Systems* 7, 1 (2023), 1–25.
- [30] Shuai Liu, Xin Li, Huchuan Lu, and You He. 2022. Multi-Object Tracking Meets Moving UAV. In *Proceedings of the IEEE/CVF Conference on Computer Vision and Pattern Recognition (CVPR)*. 8876–8885.
- [31] Weiyang Liu, Yandong Wen, Zhiding Yu, and Meng Yang. 2016. Large-margin softmax loss for convolutional neural networks. *arXiv preprint arXiv:1612.02295* (2016).
- [32] Antoni Masiukiewicz. 2019. Throughput comparison between the new HEW 802.11 ax standard and 802.11 n/ac standards in selected distance windows. *International Journal of Electronics and Telecommunications*

- 1321 65, 1 (2019), 79–84.
- 1322 [33] William McNally, Kanav Vats, Alexander Wong, and John McPhee. 2022. Rethinking keypoint representations: Modeling keypoints and poses as objects for multi-person human pose estimation. In *European Conference on Computer Vision*. Springer, 37–54.
- 1323 [34] Thaha Mohammed, Carlee Joe-Wong, Rohit Babbar, and Mario Di Francesco. 2020. Distributed inference acceleration with adaptive DNN partitioning and offloading. In *IEEE INFOCOM 2020-IEEE Conference on Computer Communications*. IEEE, 854–863.
- 1324 [35] Deepak Narayanan, Mohammad Shoeybi, Jared Casper, Patrick LeGresley, Mostofa Patwary, Vijay Korthikanti, Dmitri Vainbrand, Prethvi Kashinkunti, Julie Bernauer, Bryan Catanzaro, et al. 2021. Efficient large-scale language model training on gpu clusters using megatron-lm. In *Proceedings of the International Conference for High Performance Computing, Networking, Storage and Analysis*. 1–15.
- 1325 [36] Mohammad Noormohammadpour and Cauligi S Raghavendra. 2017. Datacenter traffic control: Understanding techniques and tradeoffs. *IEEE Communications Surveys & Tutorials* 20, 2 (2017), 1492–1525.
- 1326 [37] NVIDIA. 2024. The World’s Smallest AI Supercomputer. <https://www.nvidia.com/en-us/autonomous-machines/embedded-systems/jetson-xavier-series/>.
- 1327 [38] Takeshi Ohkawa, Kazushi Yamashina, Hitomi Kimura, Kanemitsu Ootsu, and Takashi Yokota. 2018. FPGA components for integrating FPGAs into robot systems. *IEICE TRANSACTIONS on Information and Systems* 101, 2 (2018), 363–375.
- 1328 [39] Yuanteng Pei, Matt W Mutka, and Ning Xi. 2013. Connectivity and bandwidth-aware real-time exploration in mobile robot networks. *Wireless Communications and Mobile Computing* 13, 9 (2013), 847–863.
- 1329 [40] pytorch. 2024. pytorch. <https://pytorch.org/>.
- 1330 [41] pytorch. 2024. pytorch. <https://pytorch.org/docs/stable/generated/torch.nn.Conv2d.html>.
- 1331 [42] A Kai Qin, Vicky Ling Huang, and Ponnuthurai N Suganthan. 2008. Differential evolution algorithm with strategy adaptation for global numerical optimization. *IEEE transactions on Evolutionary Computation* 13, 2 (2008), 398–417.
- 1332 [43] Yi Ren, Chih-Wei Tung, Jyh-Cheng Chen, and Frank Y Li. 2018. Proportional and preemption-enabled traffic offloading for IP flow mobility: Algorithms and performance evaluation. *IEEE Transactions on Vehicular Technology* 67, 12 (2018), 12095–12108.
- 1333 [44] Nurul I Sarkar and Osman Mussa. 2013. The effect of people movement on Wi-Fi link throughput in indoor propagation environments. In *IEEE 2013 Tencon-Spring*. IEEE, 562–566.
- 1334 [45] Karen Simonyan and Andrew Zisserman. 2015. Very Deep Convolutional Networks for Large-Scale Image Recognition. arXiv:1409.1556 [cs.CV]
- 1335 [46] Debjyoti Sinha and Mohamed El-Sharkawy. 2019. Thin mobilenet: An enhanced mobilenet architecture. In *2019 IEEE 10th annual ubiquitous computing, electronics & mobile communication conference (UEMCON)*. IEEE, 0280–0285.
- 1336 [47] Luna Sun, Zhenxue Chen, QM Jonathan Wu, Hongjian Zhao, Weikai He, and Xinghe Yan. 2021. AMPNet: Average-and max-pool networks for salient object detection. *IEEE Transactions on Circuits and Systems for Video Technology* 31, 11 (2021), 4321–4333.
- 1337 [48] Sasha Targ, Diogo Almeida, and Kevin Lyman. 2016. Resnet in resnet: Generalizing residual architectures. *arXiv preprint arXiv:1603.08029* (2016).
- 1338 [49] Hao Wang, Sreeram Potluri, Miao Luo, Ashish Kumar Singh, Sayantan Sur, and Dhabaleswar K Panda. 2011. MVAPICH2-GPU: optimized GPU to GPU communication for InfiniBand clusters. *Computer Science Research and Development* 26, 3 (2011), 257–266.
- 1339 [50] Junming Wang, Zekai Sun, Xiuixian Guan, Tianxiang Shen, Zongyuan Zhang, Tianyang Duan, Dong Huang, Shixiong Zhao, and Heming Cui. 2024. AGRNav: Efficient and Energy-Saving Autonomous Navigation for Air-Ground Robots in Occlusion-Prone Environments. In *IEEE International Conference on Robotics and Automation (ICRA)*.
- 1340 [51] Lin Wang and Kuk-Jin Yoon. 2021. Knowledge distillation and student-teacher learning for visual intelligence: A review and new outlooks. *IEEE transactions on pattern analysis and machine intelligence* 44, 6 (2021), 3048–3068.
- 1341 [52] Sanghyun Woo, Shoubhik Debnath, Ronghang Hu, Xinlei Chen, Zhuang Liu, In So Kweon, and Saining Xie. 2023. Convnext v2: Co-designing and scaling convnets with masked autoencoders. In *Proceedings of the IEEE/CVF Conference on Computer Vision and Pattern Recognition*. 16133–16142.
- 1342 [53] Huaming Wu, William J Knottenbelt, and Katinka Wolter. 2019. An efficient application partitioning algorithm in mobile environments. *IEEE Transactions on Parallel and Distributed Systems* 30, 7 (2019), 1464–1480.
- 1343 [54] Tianyu Wu, Shizhu He, Jingping Liu, Siqi Sun, Kang Liu, Qing-Long Han, and Yang Tang. 2023. A brief overview of ChatGPT: The history, status quo and potential future development. *IEEE/CAA Journal of Automatica Sinica* 10, 5 (2023), 1122–1136.
- 1344 [55] Zhaoyang Xia, Youquan Liu, Xin Li, Xinge Zhu, Yuexin Ma, Yikang Li, Yuenan Hou, and Yu Qiao. 2023. SCPNet: Semantic Scene Completion on Point Cloud. In *Proceedings of the IEEE/CVF Conference on Computer Vision and Pattern Recognition*. 17642–17651.
- 1345 [56] Yecheng Xiang and Hyoseung Kim. 2019. Pipelined data-parallel CPU/GPU scheduling for multi-DNN real-time inference. In *2019 IEEE Real-Time Systems Symposium (RTSS)*. IEEE, 392–405.
- 1346 [57] Jing Xu, Yu Pan, Xinglin Pan, Steven Hoi, Zhang Yi, and Zenglin Xu. 2022. RegNet: self-regulated network for image classification. *IEEE Transactions on Neural Networks and Learning Systems* (2022).
- 1347 [58] Min Xue, Huaming Wu, Guang Peng, and Katinka Wolter. 2021. DDPQN: An efficient DNN offloading strategy in local-edge-cloud collaborative environments. *IEEE Transactions on Services Computing* 15, 2 (2021), 640–655.
- 1348 [59] Xinlei Yang, Hao Lin, Zhenhua Li, Feng Qian, Xingyao Li, Zhiming He, Xudong Wu, Xianlong Wang, Yunhao Liu, Zhi Liao, et al. 2022. Mobile access bandwidth in practice: Measurement, analysis, and implications. In *Proceedings of the ACM SIGCOMM 2022 Conference*. 114–128.
- 1349 [60] Yang Yang, Li Juntao, and Peng Lingling. 2020. Multi-robot path planning based on a deep reinforcement learning DQN algorithm. *CAAI Transactions on Intelligence Technology* 5, 3 (2020), 177–183.
- 1350 [61] Xinyou Yin, JAN Goudriaan, Egbert A Lantinga, JAN Vos, and Huub J Spiertz. 2003. A flexible sigmoid function of determinate growth. *Annals of botany* 91, 3 (2003), 361–371.
- 1351 [62] Chaoqun Yue, Ruofan Jin, Kyoungwon Suh, Yanyuan Qin, Bing Wang, and Wei Wei. 2017. LinkForecast: Cellular link bandwidth prediction in LTE networks. *IEEE Transactions on Mobile Computing* 17, 7 (2017), 1582–1594.
- 1352 [63] Anthony Zee. 1996. Law of addition in random matrix theory. *Nuclear Physics B* 474, 3 (1996), 726–744.
- 1353 [64] Yonghao Zhuang, Hexu Zhao, Lianmin Zheng, Zhuohan Li, Eric Xing, Qirong Ho, Joseph Gonzalez, Ion Stoica, and Hao Zhang. 2023. On optimizing the communication of model parallelism. *Proceedings of Machine Learning and Systems* 5 (2023).